Proceedings of the ASME 2010 3rd Joint US-European Fluids Engineering Summer Meeting and 8th International Conference on Nanochannels, Microchannels, and Minichannels
FEDSM-ICNMM2010
August 1-5, 2010, Montreal, Canada

FEDSM-ICNMM2010-30552

LES AND RANS SIMULATION OF TURBULENT AIRFLOW AND TRACER GAS INJECTION IN A GENERIC AIRCRAFT CABIN MODEL

Khosrow Ebrahimi
Mechanical and Nuclear Engineering
Kansas State University
khe1976@ksu.edu

Zhongquan C. Zheng
Mechanical and Nuclear Engineering
Kansas State University
zzheng@ksu.edu

Mohammad H. Hosni
Mechanical and Nuclear Engineering
Kansas State University
hosni@ksu.edu

ABSTRACT

This study is a continuation of a previous research in numerical simulation of a turbulent airflow in a generic aircraft cabin model. Specifically, the primary objective of this project is to use Computational Fluid Dynamics (CFD) to simulate transport of a tracer gas injected into the generic aircraft cabin. The research work reported herein is composed of three parts.

First, both Large Eddy Simulation (LES) and Reynolds averaged Navier Stokes (RANS) methods are used to simulate airflow from a full-height nozzle and corresponding airflow characteristics within the mockup aircraft cabin. The computational results are validated by comparing them with Particle Image Velocity (PIV) data and published CFD predictions available in the literature. Through these comparisons, the potential for using the CFD methods to predict unsteady as well as time-averaged velocity for a generic aircraft cabin model is examined.

Second, airflow characteristics are studied by reducing the inlet nozzle height to one-half of its original size but keeping the total volumetric airflow rate the same as that of the full-height nozzle. Accuracy of the LES approach in predicting airflow in the half-height nozzle is evaluated by comparing prediction results with the PIV measurement data for the mockup cabin.

Third, simulation of a tracer gas injection through the injecting tube placed in different locations in the half-height nozzle cabin is investigated. In this part, carbon dioxide (CO_2) is chosen as the tracer gas. The LES method is used to solve the equations of motion and the unsteady species transport equation for tracer gas concentration. The predictions are compared with the average measurement data for CO_2-concentration in various locations in the cabin.

INTRODUCTION

Computational Fluid Dynamics has been used for a few decades to evaluate the performance of air conditioning systems through the simulation of fluid flow and heat transfer for the indoor environments. Due to the advances in the computer technology and in turbulence models, use of CFD as a powerful and economical design tool for improving the efficiency and performance of air conditioning systems has been increased. In aircraft industry, CFD models are used to investigate the effect of air ventilation system on the passenger comfort as well as the dispersion of particulates and gases as part of understanding the possible spread of contaminants within an aircraft cabin (Lebbin, 2006).

There are a number of research articles in the literature that discuss the use of CFD approaches to study the airflow and contaminants transport in aircraft cabins. Garner et al. (2004) presented a CFD model which was developed to simulate the airflow field characteristics in a Boeing 747 aircraft cabin. The applied CFD model is described by the unsteady, time-accurate, buoyant ventilation flow field in an aircraft cabin at cruise conditions. The simulation was conducted using a finite element implementation of an augmented laminar Taylor stabilized finite turbulent kinetic energy (TKE) model.

Lin et al. (2005) performed a numerical simulation of airflow and airborne pathogen transport in a commercial aircraft

cabin (Boeing 767). Two different turbulence models were used in that study; Large Eddy Simulation (LES) and Reynolds Averaged Navier Stokes (RANS) models. It was observed while RANS simulation substantially under-predicted turbulent intensity, the LES predicted values were in good agreement with the test data. Based on the LES results, the k-ε equations in the RANS model were modified and then used in simulating the disease transmission using less than 1/100 of computing resources required for the equivalent LES simulation of particle transport in the same cabin.

Lin et al. (2006) performed another study in which the CFD predicted velocity data for turbulent airflow in a generic cabin model were compared with corresponding Particle Image Velocimetry (PIV) experimental data. The main focus of that study was using LES simulation to compare the temporal variations in the experimental data. The good agreement between the simulation results and measured data validated the LES predictions. Also it was observed that energy-spectrum function calculated from the LES velocity prediction had excellent correlation with the Kolmogrov spectrum law in the universal equilibrium range.

The present study is designed to simulate the turbulent airflow and tracer gas diffusion in the same generic cabin as used in Lin et al. (2006) research. A commercial CFD software is used for simulations presented herein. In the first part of this study which deals with airflow characteristics in the cabin, two widely used turbulence models are employed: LES and RANS. The LES method provides the temporal velocity variations and the RANS procedure gives time-independent velocity data. The predictions from both the LES and RANS models are compared with the PIV measured data for five monitoring areas along the cabin center plane parallel to the bulk airflow direction (Lebbin, 2006). Through these comparisons the capability of the two aforementioned turbulence models in predicting the airflow velocities is discussed and compared to each other.

In the second part of this study, the effect of reducing the inlet nozzle height to one-half of its original size on turbulence level and airflow velocities is studied, while maintaining the same Reynolds number for inlet airflow. In this part the predictions are validated by comparing them with the corresponding experimental PIV measurements. In the third part of this study, the tracer gas (CO2) injection is simulated using the LES model for solving the governing mass, momentum and transport species equations. The simulation results are validated through the comparison of time-averaged predicted concentrations of the tracer gas in specified locations in the cabin with the corresponding experimental measurements.

GOVERNING EQUATIONS AND NUMERICAL SOLUTION METHOD

In this study the following assumptions are employed for numerical simulation of turbulent airflow and tracer gas injection in the cabin. Theses assumptions conform to the experimental conditions. The assumptions are:

1. The airflow field is 3-dimensional.
2. In the LES model, the flow is considered unsteady while in the RANS model, the flow is assumed to be at steady state conditions.
3. In both cases of pure airflow and air-CO_2 mixture, the fluid is assumed to be incompressible.
4. The heat transfer in the cabin is neglected. The inlet airflow is at the temperature of 27^{o}C. In simulating the carbon dioxide diffusion, the temperature of injected CO_2 is also considered to be at 27^{o}C.
5. In simulating the tracer gas injection, the effects of buoyancy are taken into account.
6. No chemical reaction takes place in tracer gas diffusion.

The governing equations of turbulent airflow in the cabin are listed as follows:

Continuity:

$$\frac{\partial u_i}{\partial x_i} = 0 \qquad (1)$$

Momentum (Navier-Stokes equations):

$$\frac{\partial u_i}{\partial t} + u_j \frac{\partial u_i}{\partial x_j} = -\frac{1}{\rho}\frac{\partial p}{\partial x_i} + \frac{1}{\rho}\frac{\partial}{\partial x_j}\left(\mu \frac{\partial u_i}{\partial x_j}\right) + g_i \qquad (2)$$

In solving the above equations using LES, just the large scale motions of the flow are solved by filtering out the small and universal eddies. In other words, in this approach the velocity field is separated into resolved and sub-grid domains. The resolved domain of the velocity field represents the large eddies which are dependent on the geometry while the sub-grid domain represents the small scale eddies which are not dependent on the geometry of flow and have a universal behavior such that their effect on the resolved domain is included through the sub-grid scale (SGS) model. So, in this method the instantaneous velocity is considered as the summation of resolvable scale velocity ($\widetilde{u}_i$) and sub-grid scale velocity (u_i''):

$$u_i = \widetilde{u}_i + u_i'' \qquad (3)$$

It should be mentioned that in the most commercial CFD packages, the grid size is used to filter out sub-grid scale eddies. Substituting the decomposition forms of u_i (as indicated by Equation-3) and p ($p = \widetilde{p} + p''$) in the instantaneous governing continuity and Navier-Stokes equations, and then filtering the resulting equations, gives the following filtered equations of continuity and motion:

$$\frac{\partial \tilde{u}_i}{\partial x_i} = 0 \quad (4)$$

$$\frac{\partial \tilde{u}_i}{\partial t} + \tilde{u}_j \frac{\partial \tilde{u}_i}{\partial x_j} = -\frac{1}{\rho}\frac{\partial \tilde{p}}{\partial x_i} + \frac{1}{\rho}\frac{\partial}{\partial x_j}\left([\mu + \mu_t]\frac{\partial \tilde{u}_i}{\partial x_j}\right) + g_i \quad (5)$$

where μ_t in Equation (5) is the sub-grid scale turbulent viscosity. In this study, the Smagorinsky-Lilly SGS model (Smagorinsky, 1963 and Lilly, 1966) is used to calculate μ_t:

$$\mu_t = \frac{\rho}{\sqrt{2}}(C_s\Delta)^2\left|\frac{\partial \tilde{u}_i}{\partial x_j} + \frac{\partial \tilde{u}_j}{\partial x_i}\right| \quad (6)$$

where Δ is the filter width and can be calculated using the following equation:

$$\Delta = (\text{Volume of the grid element})^{1/3} \quad (7)$$

and C_s is the Smagorinsky constant which varies between 0.1 and 0.2. In this study the selected value for C_s is 0.14.

As was mentioned earlier, the heat transfer is negligible in the cabin so that the energy or heat equation is not needed. Needless to say, the governing equations are second order with respect to space and first order with respect to time, so that in solving the governing equations we need to have two boundary conditions in each direction and one initial condition.

When the RANS models are used to simulate the turbulent airflow in the cabin, the instantaneous flow variables are decomposed into the mean value (time-averaged) and fluctuating components:

$$u_i = \bar{u}_i + u_i' \quad (8)$$

where $\bar{u}_i$ and u_i' denote the mean and fluctuating components of the flow velocity, respectively. Substituting the decomposed form of flow variables in the instantaneous governing equations (2) and (3) and taking a time average of those equations gives the following time-averaged governing equations for the steady state incompressible flow:

$$\frac{\partial \bar{u}_i}{\partial x_i} = 0 \quad (9)$$

$$\frac{\partial \bar{u}_j \bar{u}_i}{\partial x_i} = \frac{\partial}{\partial x_i}\left(-\bar{p}\delta_{ij} + (\mu + \mu_t)\left(\frac{\partial \bar{u}_i}{\partial x_j} + \frac{\partial \bar{u}_j}{\partial x_i}\right)\right) + \rho g_i \quad (10)$$

where μ_t is the turbulent or eddy viscosity and using the Boussinesq hypothesis, is defined as:

$$\mu_t = \frac{-\rho\overline{u_i' u_j'}}{\frac{\partial \bar{u}_i}{\partial x_j} + \frac{\partial \bar{u}_j}{\partial x_i}} \quad (11)$$

In this study, in order to calculate the above defined turbulent viscosity, the $k-\varepsilon$ model which is a typical two equation turbulence model is employed. Using this model, the turbulent viscosity is calculated through the following equation (Tu et al., 2008):

$$\mu_t = \frac{C_\mu \rho k^2}{\varepsilon} \quad (12)$$

where $C_\mu = 0.09$ is an empirical constant, k and ε denote the turbulent kinetic energy and turbulent dissipation. Therefore, in addition to the time-averaged governing equations, two additional differential transport equations are solved (along with required boundary conditions) at the same time to find k and ε.

To simulate the carbon dioxide diffusion in the cabin, the LES is used as the turbulence model. In this part of study, not only the geometry of the cabin is changed due to locating the carbon dioxide injection tube in the cabin, but also the equation for transport of species is added to the governing equations:

$$\frac{\partial(\rho\tilde{Y})}{\partial t} + \frac{\partial}{\partial x_i}\left(\rho\tilde{u}_i\tilde{Y}\right) = -\frac{\partial}{\partial x_i}\left(-(\rho D + \frac{\mu_t}{Sc_t})\frac{\partial \tilde{Y}}{\partial x_i}\right) \quad (13)$$

In the above equation, $\tilde{Y}$ is the carbon dioxide mass fraction in the resolved domain of eddies in the air-CO_2 mixture, D is the diffusion coefficient of carbon dioxide in the air-CO_2 mixture. In this study, it is assumed that the estimated value for $D = 1.57\times10^{-5} m^2/s$ is constant throughout the simulations (Bird el al., 2001). The turbulent Schmidt number is defined as $Sc_t = \frac{\mu_t}{\rho D_t}$, where D_t is the turbulent diffusion coefficient. In the simulations we selected Sc_t=0.7. Since Eq. (13), in terms of $\tilde{Y}$, is second order with respect to space and first order with respect to time, we need to determine two boundary conditions for $\tilde{Y}$ in each direction and one initial condition.

Another important point is that the viscosity and density of the air-carbon dioxide mixture are not uniformly constant in the cabin and their values in each location in the cabin are dependent on the concentration of constituents at that location. There are a number of methods in the commercial software to calculate the density and viscosity in a mixture. In this study the "volumetric-weighted mixing law" and "mass weighted mixing law" are used to calculate the mixture density and viscosity, respectively, as presented below:

Volumetric Weighted Mixing law:

$$\frac{1}{\rho_{mixture}} = \frac{\tilde{Y}}{\rho_{CO_2}} + \frac{1-\tilde{Y}}{\rho_{air}} \quad (14)$$

Mass Weighted Mixing law:

$$\mu_{mixture} = \tilde{Y}\mu_{CO_2} + (1-\tilde{Y})\mu_{air} \qquad (15)$$

So it can be seen that in order to simulate the tracer gas diffusion in the cabin, Equations (4-6) and (13-15) are solved simultaneously with the determined boundary and initial conditions.

To solve the above governing equations using LES method, the second order central differencing as well as the second order implicit schemes are used to discretize spatial and temporal derivatives, respectively. Also in this method, Werner-Wengle wall function (Werner and Wengle, 1991) is used as the near wall approach. The reason for using Werner-Wengle wall function for the near wall treatment, as explained elaborately by Werner and Wengle (1991), is its simplicity as well as its more accuracy in comparison with the other wall functions. While other functions are multi-domain functions based on non-dimensionalized velocity and distance from the wall, Werner-Wengle wall function defines unique relationships between shear stress and velocity that enhances accuracy and reduces the computational time. In the RANS method, the second order upwind scheme is used to discretize spatial derivatives in the governing equations. Two different wall approaches are selected: the enhanced wall treatment and non-equilibrium wall function, for the near wall treatment in the RANS method.

RESULTS AND DISCUSSIONS

Part 1- Study of airflow in cabin with full height nozzle

This section starts with the Large Eddy Simulation of turbulent airflow in the generic cabin with the full-height nozzle. The geometry of the cabin as well as the location of PIV measuring windows are shown in Fig. 1:

The generic cabin model has the key features of one-half of a twin-aisle aircraft cabin. The upper left and upper right corners represent the overhead bins. The slit right below the upper left corner represents the nozzle port through which the fresh conditioned air comes into the cabin and the slit in the lower right corner represents the outlet port for exiting exhaust air.

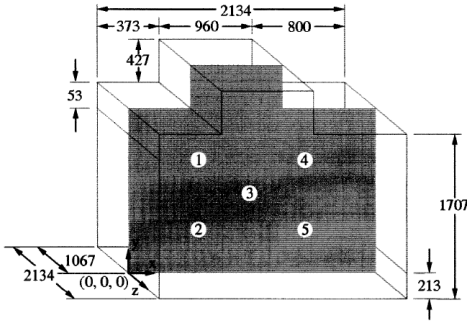

Figure 1: Simplified generic cabin model and the location of PIV monitoring windows on the cabin central plane (units in mm). (Lebbin, 2006)

In the experiment, the adiabatic condition was assumed for the cabin and the measurements were taken at five measurement locations when the airflow inside the cabin was fully developed (Lebbin, 2006), as shown in Fig. 2.

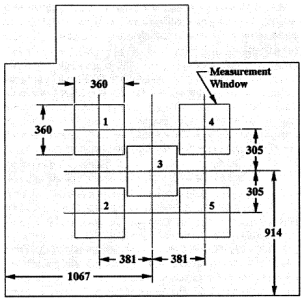

Figure 2: The exact locations of five PIV measurement windows on the central plane (units in mm). (Lin et al., 2006)

In the experiments, the average airflow rate coming into the cabin was maintained at the constant value of 4.2 m^3/min. The Reynolds number at the inlet was held constant at 2,226. In LES, the spacing of the mesh has a very important role in the quality and the accuracy of simulation predictions not only because of using that in discretizing the governing equations but also because it is used in filtering the instantaneous governing equations. Another important parameter affecting the accuracy of simulations is the size of the time steps. Knowing the Reynolds number at the inlet, the Kolmogrov length (η) and time (τ) scales are calculated as 0.928 mm and 0.0589 sec., respectively. Although the Kolmogrov length and time scales are used as a basis in the grid and time spacing, making a decision on the grid and time spacing requires a compromise between the solution accuracy, the computation time and cost as well as the existing restrictions in the computing resources. The CFD grid used in this part of study consists of 2,340,000 hexahedral cells with the grid spacing varied in the range of 7η - 34η. Also the time step size of 0.05 sec is used in all Large Eddy Simulations presented in this paper.

Figure 3 shows the turbulent airflow patterns in the cabin at four different time levels predicted using LES. This sequence

also shows the development of the flow field inside the cabin, such as formation of boundary layers and large eddies.

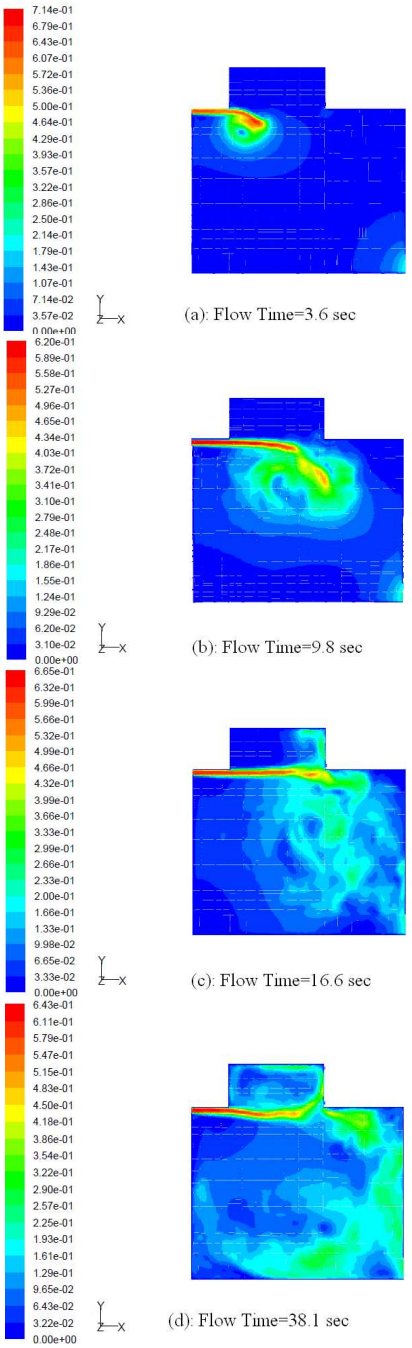

Figure 3: The turbulent airflow patterns (The contour representations of airflow velocity magnitudes) predicted by LES at different flow times: (a) flow time=3.6 s, (b) flow time=9.8 s, (c) flow time=16.579 s and (d) flow time=38.1 s (units in m/s).

In order to validate the simulation, the LES predictions are compared with the PIV measurement data as well as the CFD predictions by Lin et al. (2006) at each of the five PIV measuring areas. The PIV measurements were taken when the airflow inside the cabin reached quasi-steady conditions. The time interval between each two succeeding PIV sampling data was 0.2 sec (Lebbin, 2006). A comparison between the corresponding LES parameters used in this study and those used in Lin et al. (2006) is listed in Table 1.

We first consider the value of velocity at the center point of each PIV measuring windows as the measured value of velocity in that window, as assumed by Lin et al. (2006). The predicted temporal histories of velocity components at these points are compared with the PIV data obtained with a sampling frequency of 5 Hz, as well as the CFD predictions by Lin et al (2006) that had a sampling frequency of 20 Hz. Figures 4-6 show some of those comparisons for the locations 1 and 4. Since the values of z-component of airflow velocities in the central cutting plane (z=0) is so small, just the comparisons for x and y components of airflow velocities are presented here.

Table 1: Comparison between the important parameters in the simulations

LES CODE	Lin et al. (2006) (Using Commercial CODE)	Lin et al. (2006) (Using Fire Dynamic Simulator)	This Study (Using Commercial Software)
Mesh size (# of cells)	2,553,744	2,580,480	2,340,000
Cell Type	All hexahedral cells, unstructured mesh	All hexahedral cells, Cartesian Mesh	All hexahedral cells, Structured mesh
Grid Spacing(η)	5-20	5-20	7-34
Time Step(seconds)	0.05	0.01 ± 0.002	0.05
SGS model	Smagorinsky Lilly	Smagorinsky Lilly	Smagorinsky Lilly
Smagorinsky constant, C_s	0.14	0.14	0.14
Near Wall Treatment	Law of the wall approach	Standard Wall function	Werner-Wengle
Numerical Scheme	Spatial: Second order central differencing Temporal: Implicit second order predictor corrector scheme	Spatial: Second order central differencing Temporal: Implicit second order predictor corrector scheme	Spatial: Second order central differencing Temporal: Implicit second order predictor corrector scheme

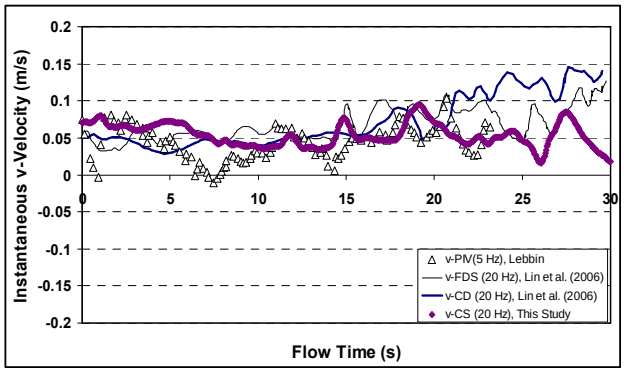

(a): x-component of velocity data

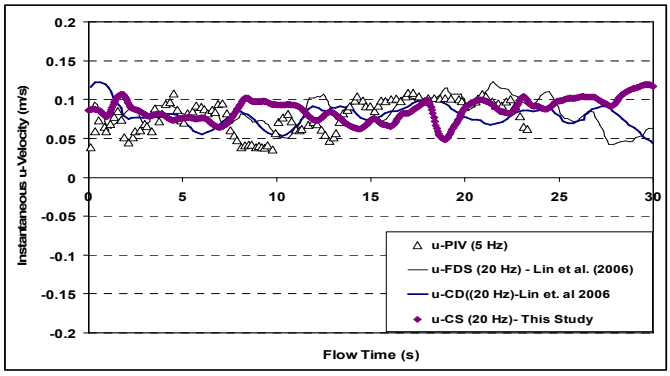

(b): y-component of velocity data

Figure 4: Comparison of the predicted values (this study), PIV measurements (Lebbin, 2006) and Lin et al (2006) predictions (using FDS and a commercial software) for the airflow velocity data corresponding to the location 1 of the cabin with full height nozzle.

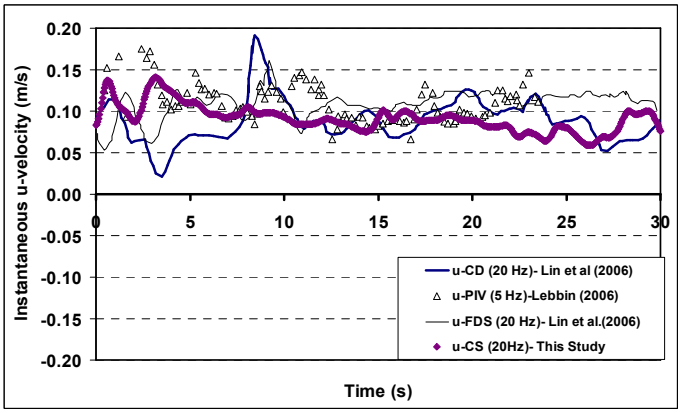

(a): x-component of velocity data

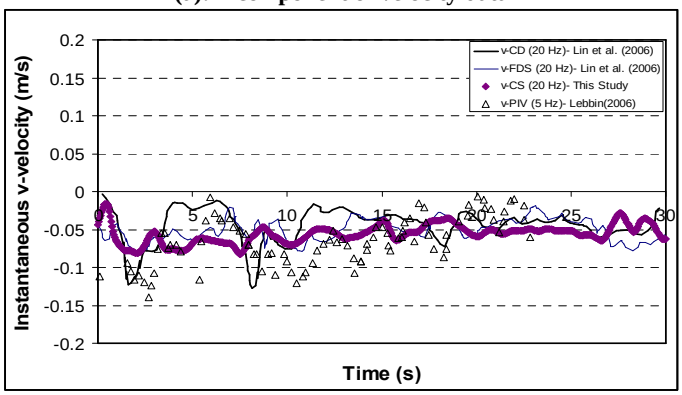

(b): y-component of velocity data

Figure 5: Comparison of the predicted values (this study), PIV measurements (Lebbin, 2006) and Lin et al (2006) predictions (using FDS and a commercial software) for the airflow velocity data corresponding to the location 4 of the cabin with full height nozzle.

As can be seen from Figs. 4-6, there is a good agreement among the simulation results of this study, PIV measurements, and Lin et al (2006) CFD predictions. Especially, the comparisons indicate that the simulations predict the ranges of variations of instantaneous velocities fairly close to the variation ranges of the measurements.

In the above comparison, the predicted velocity values were selected at the center of each PIV measuring window. However in the experiments, the PIV velocity data were averaged over the area of each measuring window. In order to study the effect of changing the prediction velocity from the center point value to the area average value of the PIV measuring windows, the simulation results were reprocessed based on the area weighted average values of velocities over the measuring windows areas. Figure 6 shows the comparisons between the predictions from two differently processed velocity values and the corresponding experimental data for location 2 of the PIV window.

In Fig. 6, it is observed that although the mean temporal behaviors of the predictions are almost the same between the two different simulation data sets, the area-averaged data set shows a smoother curve, which means the area-averaged velocity experiences less fluctuations than the local velocity at the center point of the window.

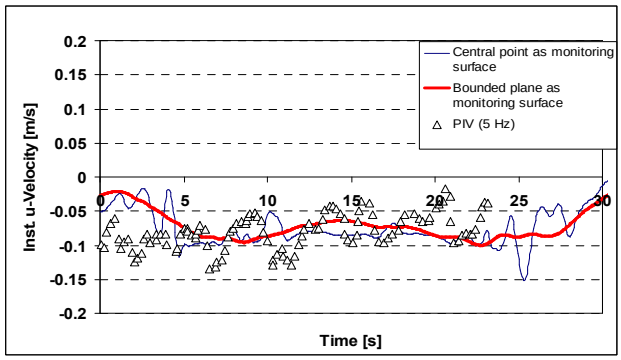

(a) x- component of velocity data

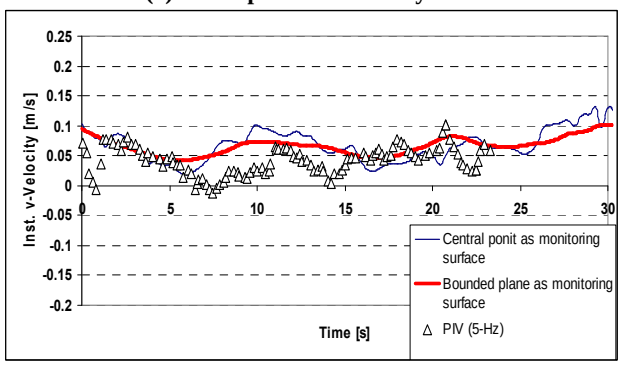

(b) y- component of velocity data

Figure 6: Study the effect of choosing monitoring surface on the predicted velocities, corresponding to location 2 of the cabin with full height nozzle, through comparison with PIV measurements.

Figures 7 and 8 present the comparisons between the predictions from the steady-state RANS simulations using three

variations of the k-ε turbulence models for the x-component of velocity in locations 3 and 5 of the PIV windows and the corresponding time-dependent PIV data. Although the accuracy of RANS predictions is considerably less than LES, the computation time and cost associated with LES simulations are much more than RANS.

Among the three examined RANS models, the standard $k-\varepsilon$ (Launder and Spalding, 1972), the re-normalization group (RNG) $k-\varepsilon$ (Yakhot and Orszag, 1986) and the realizable $k-\varepsilon$ (Shin et al., 1995), the RNG predicted value is closer to the mean value of the experimental data. The standard $k-\varepsilon$ predicted value is less than the measured mean value; however, the RNG and realizable $k-\varepsilon$ predicted values are greater than measured mean values. Based on the simulations performed in this study, the RNG is the most accurate model.

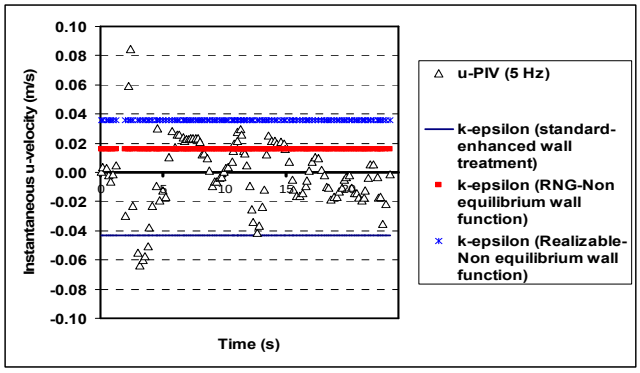

Figure 7: Comparison between the RANS predictions of time independent x-component velocity data in location 3 of measuring windows and corresponding time dependent PIV data.

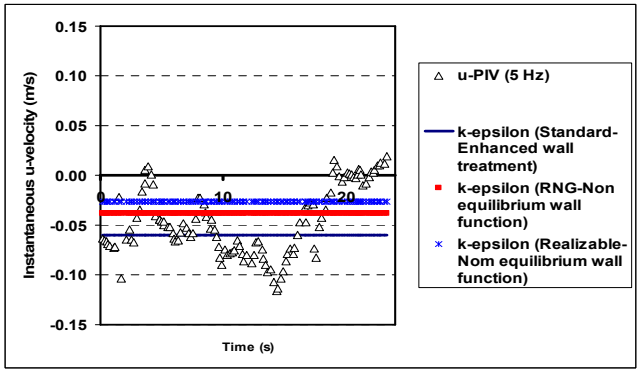

Figure 8: Comparison between the RANS predictions of time independent x-component velocity data in location 5 of measuring windows and corresponding time dependent PIV data.

Part 2- Study of the airflow in cabin with half height nozzle:

This section presents the study of flow characteristics when the cabin nozzle height is reduced to one half of its previous size. As the flow rate of the incoming air to the cabin still remains the same, by halving the nozzle height, the magnitude of the airflow velocity at the inlet is doubled. So it is expected that the magnitude of each airflow velocity component in the cabin experience an increase. Figures 9-12 compare the PIV measurements (Lebbin, 2006) with the LES predictions from this study for the airflow velocity components in location 1, 2, 3 and 5 of the PIV measuring windows. The sampling frequency in PIV measurements is 7.5 Hz. A structured grid consisting of 2,225,000 hexahedral mesh cells with the grid spacing in the range of 4η-43η was used in the LES simulations for this part of study. Similar to the simulations done for the cabin with full height nozzle, the time-step size of 0.05 sec was used in simulating the airflow in the cabin with half-height nozzle as well. As can be seen from the comparison, except for the location 3 of the measuring windows, LES predicts the range of flow velocity variations fairly well. In location 3, due to the complexity of flow in this region, the agreement between the LES predictions and PIV measurements is not as good for all flow times. For example, in Fig. 11, for the times between ~12 sec to ~30 sec and greater than ~35 sec there is not an acceptable agreement between LES and PIV. It seems in order to get better predictions for such regions in which the airflow patterns are more complicated, local grid refinements are needed.

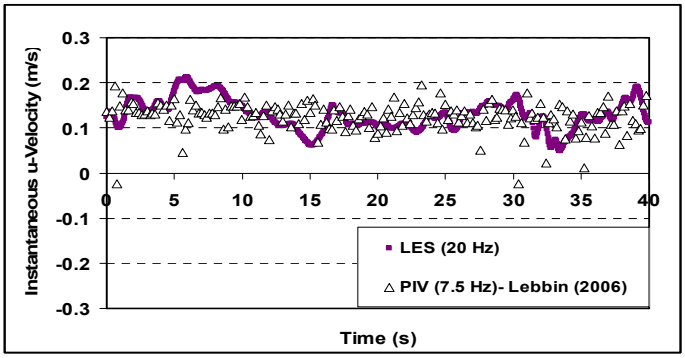

(a): x-component of velocity data

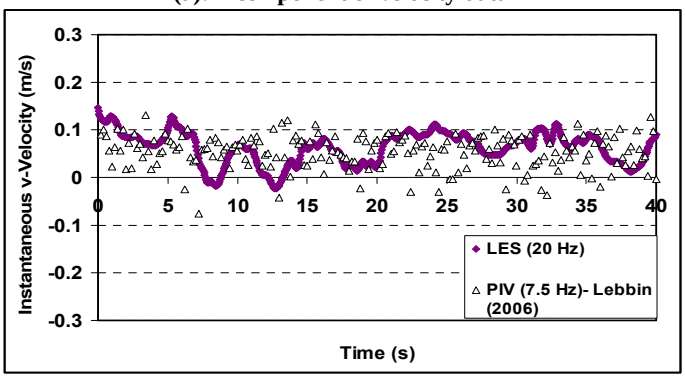

(b): y-component of velocity data

Figure 9: Comparison of the LES prediction and PIV measurements (Lebbin, 2006) for velocity data corresponding to the location 1 of the cabin with half height nozzle.

Comparisons of velocity data between the full and half height nozzle cases indicate that by halving the nozzle height,

the mean value of the predicted as well as measured flow velocity data corresponding to locations 1 and 2 of the PIV measuring windows are approximately doubled. However for the locations 4 and 5, the expected increase in the velocity is slight and not as much as that experienced in the locations 1 and 2. In addition, comparison of the PIV measurements for the velocity data corresponding to the location 3 (Fig. 13) implies that by halving the nozzle height and consequently doubling the inlet airflow velocity, the flow in the location 3, which used to be almost stationary in the full height nozzle case, takes the tendency of moving to the upper left corner of the cabin.

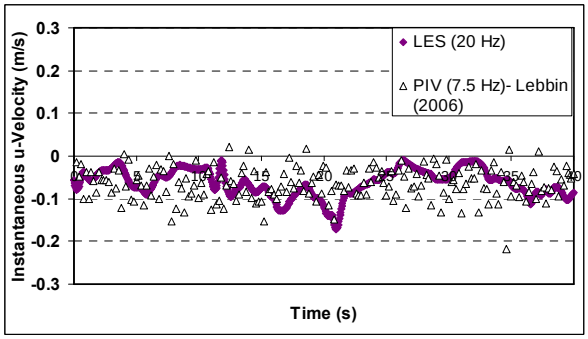

(a): x-component of velocity data

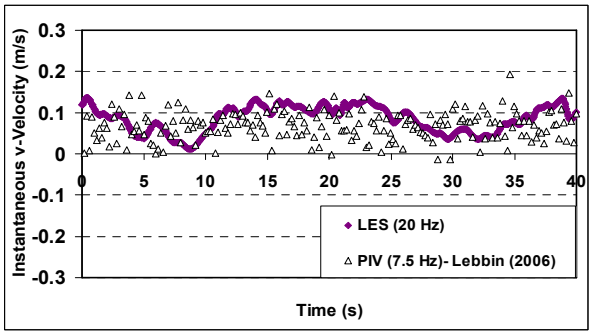

(b): y-component of velocity data

Figure 10: Comparison of the LES prediction and PIV measurements (Lebbin, 2006) for velocity data corresponding to the location 2 of the cabin with half height nozzle.

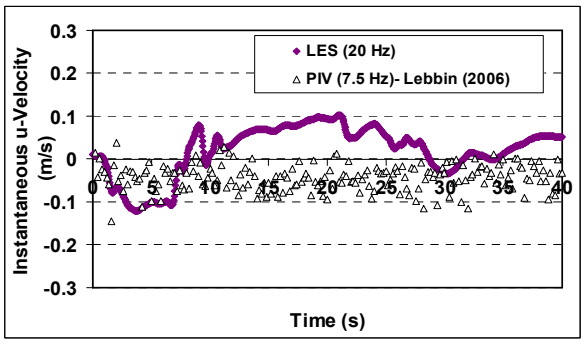

(a): x-component of velocity data

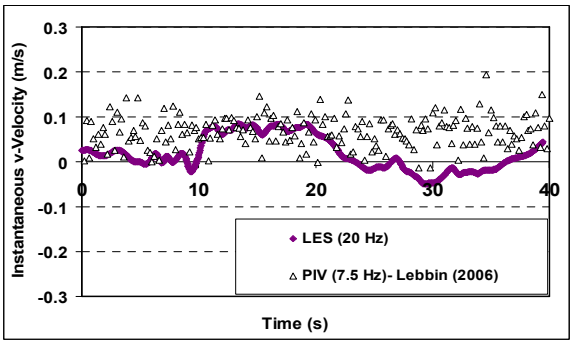

(b): y-component of velocity data

Figure 11: Comparison of the LES prediction and PIV measurements (Lebbin, 2006) for velocity data corresponding to the location 3 of the cabin with half height nozzle.

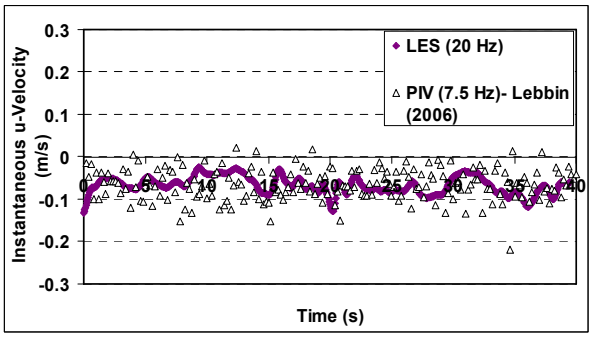

(a): x-component of velocity data

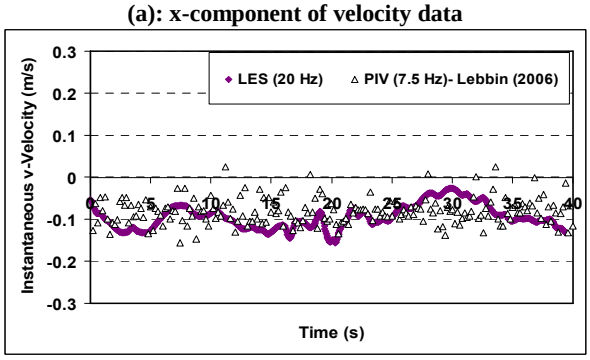

(b): y-component of velocity data

Figure 12: Comparison of the LES prediction and PIV measurements (Lebbin, 2006) for velocity data corresponding to the location 5 of the cabin with half height nozzle.

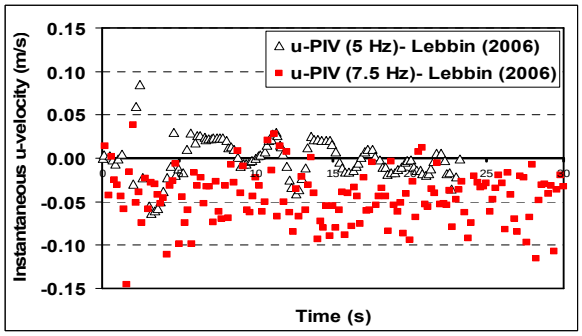

(a): x-component of velocity data

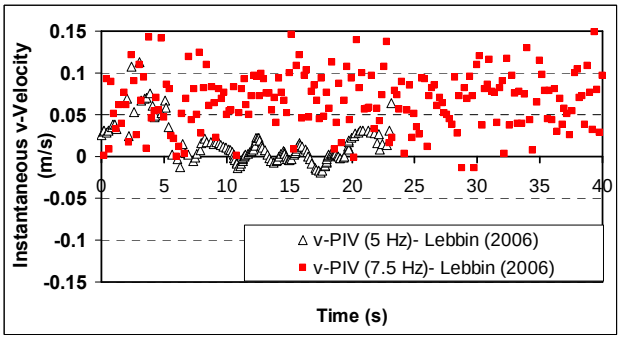

(b): y-component of velocity data

Figure 13: Study the effect of decreasing the cabin nozzle height through a comparison between the PIV measured velocity data (Lebbin, 2006) corresponding to the location 3 of the PIV measuring windows for two cases of full (PIV-5 Hz) and half nozzle height (PIV-7.5 Hz).

Part 3-Study of the tracer gas diffusion in the cabin with half height nozzle

This section is devoted to the study and understanding of the patterns of pollutants diffusion in a mockup aircraft cabin and its impact on the cabin indoor environment. In the experiments performed by Lebbin (2006), a 12.7 mm schedule-40 porous polythene tube was installed horizontally inside the cabin perpendicular to the x-y plane. One end of the tube was connected to a CO_2 tank through the back wall (corresponding to z=-1.067m) of the cabin while the other end was caped and positioned 134 mm from the opposite wall. The tube passed through the central point of the location 2 of the PIV measuring windows as identified in Figure 2. A pressurized CO_2 tank (p~800 psi containing CO_2 with the purity of more than 99.6%) was used to supply the carbon dioxide required for the experiments. By passing through an expansion valve, the pressure of carbon dioxide was regulated down from ~800 psi to an atmospheric pressure. Since the density of CO_2 at the atmospheric pressure is higher than the air density at the same pressure and temperature, in order to maintain the neutral buoyancy condition, before flowing into the injection tube, CO2 was blended with Nitrogen such that the density of the diluted CO_2 in the injection tube reached approximately the density of air. Carbon dioxide was injected through small holes uniformly distributed over the circumferential surface of the injection tube.

Figure 14 shows a rough graphical representation of the generic cabin model with the installed injection tube. In specifying the boundary conditions required for the numerical solution of the transport species equation, the concentration of the carbon dioxide in the incoming air, which is in the range of ~300 ppm to ~400 ppm, should be taken into consideration. In the experiments, the CO_2 was injected after quasi steady conditions were achieved for the turbulent airflow in the cabin. Also the measurement of the carbon dioxide concentration was performed when the flow of air-CO2 mixture reached quasi steady state conditions.

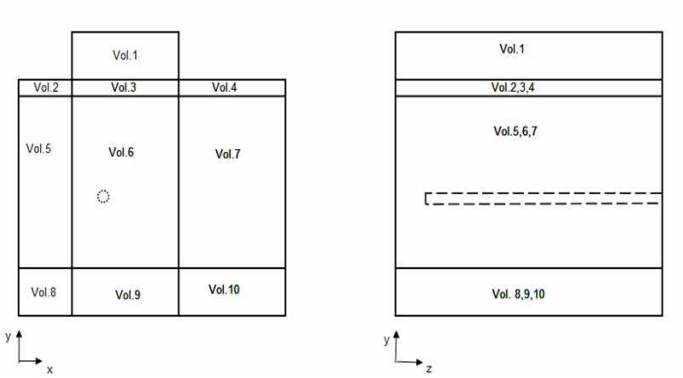

Figure 14: Rough graphical representation of the configuration of the generic cabin model and installed injection tube. (The numbered volumes indicated in the above sketch where used in grid generation for the geometry of the generic cabin model and the injection tube.

After the turbulent flow of the air-CO_2 mixture reached quasi-steady state conditions, the measurement of the time-dependent values of carbon dioxide concentration at specified sampling points, as shown in Fig.15, was started and continued for about 10 minutes. The measured data, denoted by C(t), were non-dimensionalized using the concentration of CO_2 at the inlet of the cabin and the average value of the CO_2 concentrations at the outlet between two times: at the beginning of the measurement and at the end of the measurement through the following equation:

$$y(t) = \frac{C(t) - \overline{C}_{inlet}}{\overline{C}_{outlet} - \overline{C}_{inlet}} \qquad (16)$$

where;

$y(t)$: dimensionless concentration of carbon dioxide

$C(t)$: temporal data of CO_2 concentration at different sampling points

$\overline{C}_{inlet}$: the CO_2 concentration at the inlet measured one time and assumed to be constant during the experiment

$\overline{C}_{outlet}$: the average of the two measured values for the CO_2 concentration at the outlet (the measured values are corresponded to the beginning and the end of measurement duration).

The grid generation for this geometry was performed by dividing the whole volume of the cabin model into 10 sub-volumes, as shown in Fig. 14, and producing grid for the each of theses 10 sub-volumes separately. The generated grid is unstructured and contains 1,728,000 mesh elements of tetrahedral, hexahedral and wedge shapes. A schematic of this grid is shown in Fig. 16.

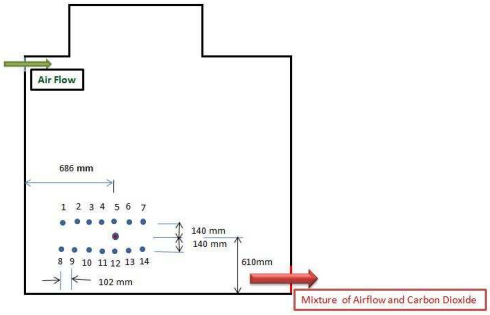

Figure 15: Points 1-14 are the sampling points above and below the injection tube. The concentration values of CO_2 are predicted using LES at these points and compared with the corresponding experimental data for CFD validation purposes.

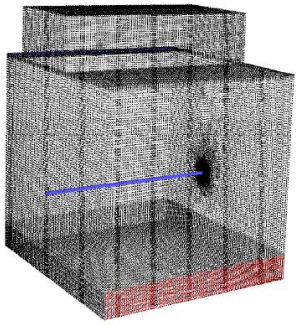

Figure 16: A 3-D schematic of the unstructured grid (for the generic cabin with the injection tube) used in CFD simulation of the carbon dioxide diffusion in the generic cabin model.

Figures 17 and 18 show comparisons between the LES predicted values for the time dependent concentration data and the corresponding time-averaged experimental measurement for the sampling points above and below the injection tube, respectively.

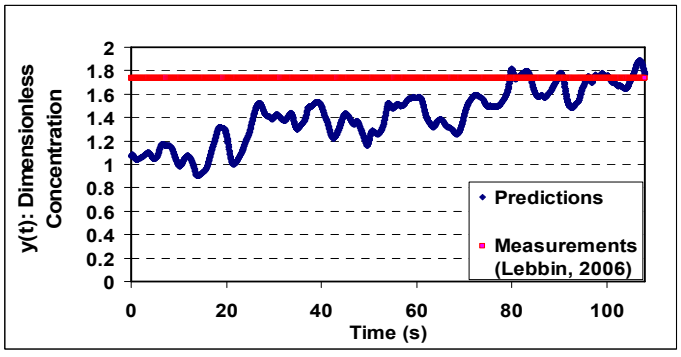

(a) Sampling point 1

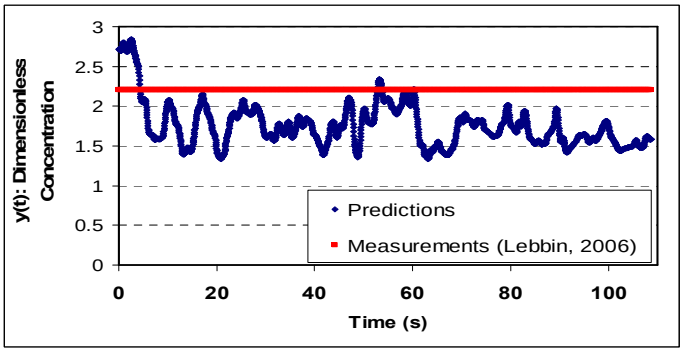

(b): Sampling point 2

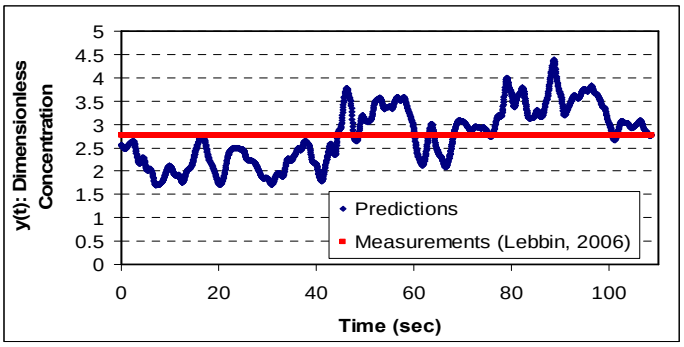

(c): Sampling point 3

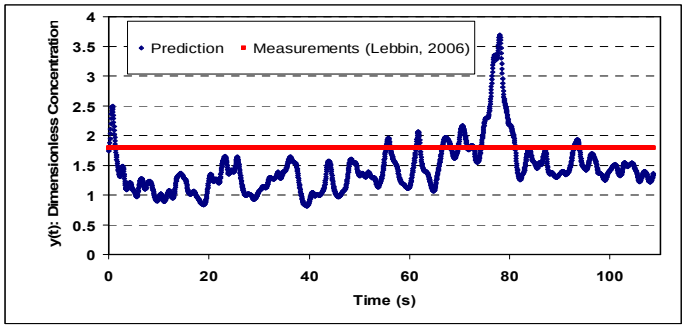

(d): Sampling point 7

Figure 17: Comparison between the time dependent predictions and time-averaged measurement for the dimensionless CO_2 concentration data at some sampling points above the injection tube (arbitrary selected).

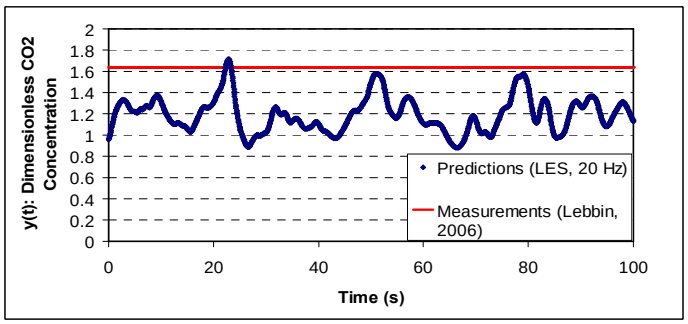

(a) Sampling point 8

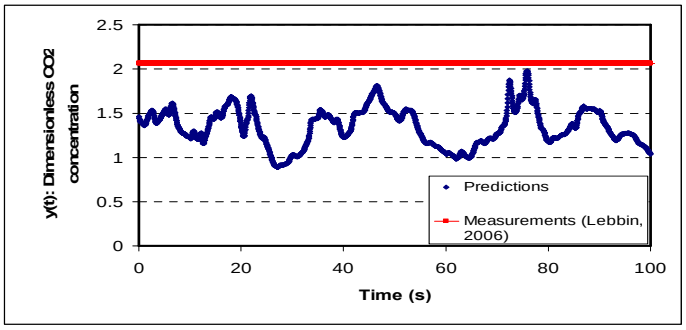

(b) Sampling point 10

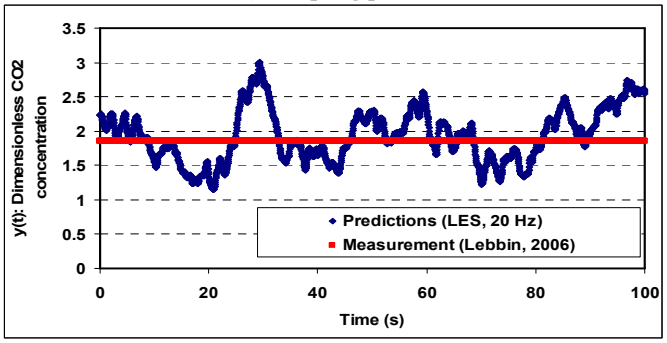

(c) Sampling point 12

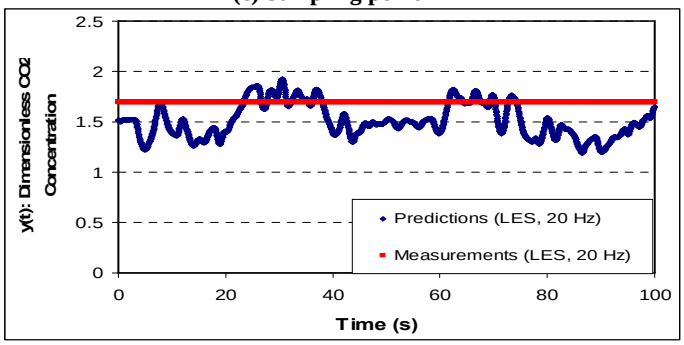

(d) Sampling point 14

Figure 18: Comparison between the time dependent predictions and time-averaged measurement for the dimensionless CO_2 concentration data at some sampling points above the injection tube (arbitrary selected)

In Figs 19 and 20, the time-averaged predicted and measured values of the CO_2 concentration are compared to each other. For the sampling points above the tube, it is observed that there is an excellent agreement between predictions and measurements at sampling points 3, 5 and 6 above the injection tube. However, the agreement for the sampling point 4 is not as good. There is an error between 11-30% in predicting the concentration data for the sampling points 1, 2 and 7 (Fig. 19)

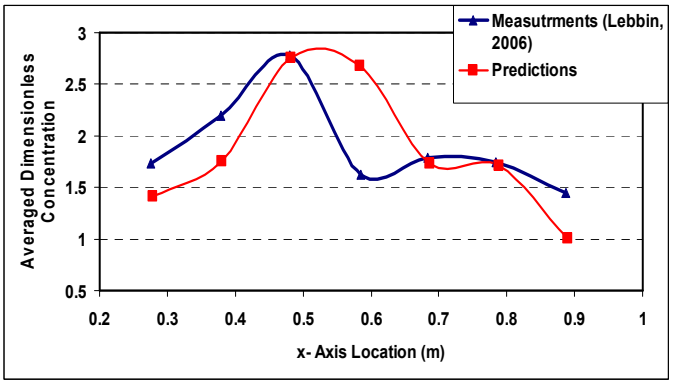

Figure 19: Comparison between the times averaged predictions and measurement of dimensionless CO_2 concentration data for the sampling points located along the x-axis above the injection tube.

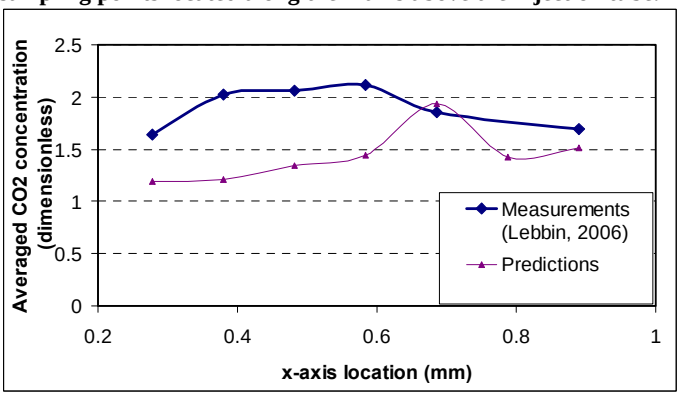

Figure 20: Comparison between the times averaged predictions and measurement of dimensionless CO_2 concentration data for the sampling points located along the x-axis above the injection tube

Figure 20 presents a graphical comparison between the time-averaged predictions and measurements for CO_2 concentration corresponding to the sampling point located along the x- axis below the injection tube. As can be seen, the best agreements have been achieved for point 12 (right below the tube) and point 14. The worst results correspond to points 8, 9 and 10. The error in computations for this case varies from ~4% (point 12) to ~40% (point 9).

Uncertainty (mesh error) study

In order to study the effect of grid size on the simulation results, the number of mesh cells was increased from 1,728,000 to 2,630,000. The CO_2 mass fraction at different sampling points computed using two different grid sizes were compared. Figure 21 shows this comparison for the sampling points above the injection tube, points 1-7 as shown in Fig. 15.

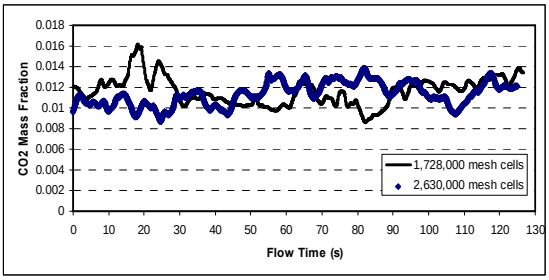

(a) Sampling point 1

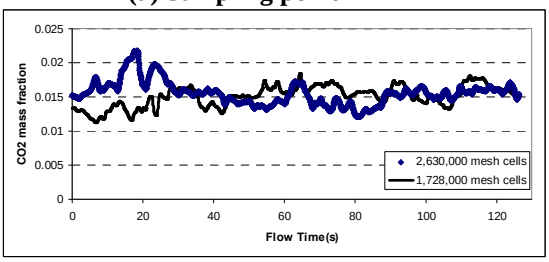

(b) Sampling point 2

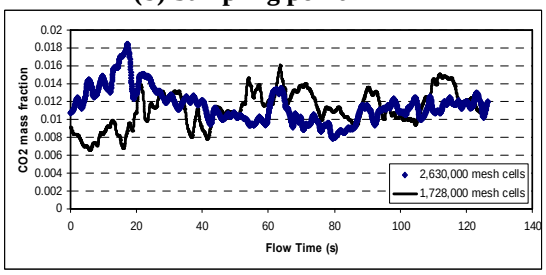

(c) Sampling point 3

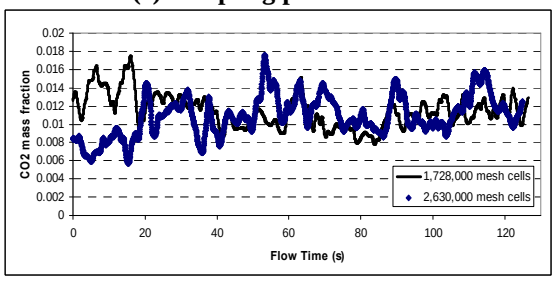

(d) Sampling point 4

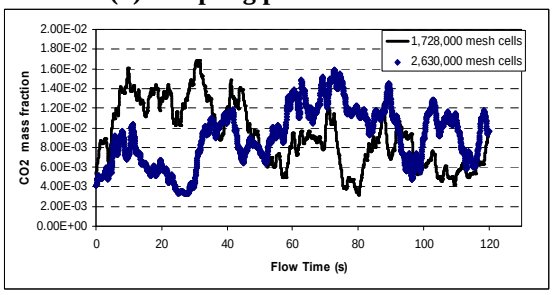

(e) Sampling point 5

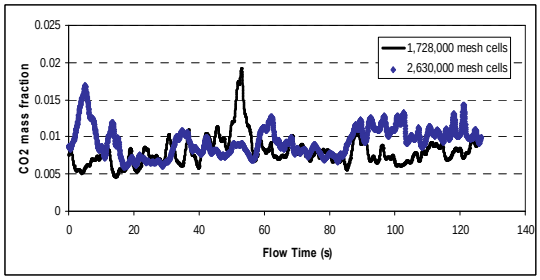

(f) Sampling point 6

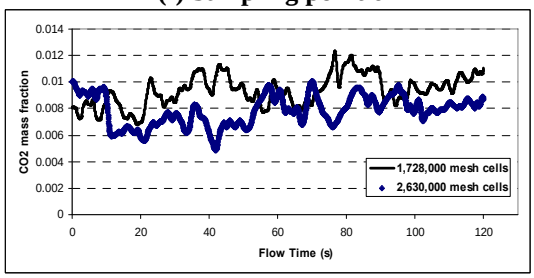

(g) Sampling point 7

Figure 21: Uncertainty (mesh error) study for simulating tracer gas injection through monitoring the CO_2 concentration at different sampling points above the injection tube.

A comparison of the root-mean-squared (RMS) values of computed data from two different grid sizes is shown in Table 2. As it is seen, by increasing the number of mesh cells, the computed CO_2 concentration data varies between 1% to 16%.

Table 2: Comparison of RMS values for computed CO_2 concentrations using two different grid sizes

Sampling point Number (Fig.15)	2,630,000 mesh cells	1,728,000 Mesh cells	Relative difference (%)
1	0.0114	0.0116	2.38
2	0.0151	0.0155	2.87
3	0.0117	0.0114	2.85
4	0.0111	0.0116	4.16
5	0.0097	0.0088	10.22
6	0.0095	0.0082	16.06
7	0.0079	0.0094	15.9

Table 3 shows comparisons between the mean values of computed data from two different grid sizes. As it is seen, by increasing the number of mesh cells, the computed CO_2 concentration data varies between 2% to 17%.

Table 3: Comparison of mean values for computed CO_2 concentrations using two different grid sizes

Sampling point Number (Fig.15)	2,630,000 mesh cells	1,728,000 Mesh cells	Relative difference %
1	0.0113	0.0116	2.08
2	0.0155	0.0151	2.89
3	0.0115	0.0112	2.85
4	0.0109	0.0114	4.86
5	0.0083	0.0092	9.78
6	0.0095	0.0082	17.1
7	0.0078	0.0093	16.13

As seen from the prediction data presented in Tables 2 and 3, the relative difference between the predicted CO_2 concentration data using two grid sizes is greater for the sampling points located in the upper right of the injection tube. In order to explain the reason for this behavior, recall the study of the airflow in the cabin presented earlier in this paper. It was observed that the airflow in the location 3 of the PIV windows (see Fig. 1) demonstrates more complexity than other locations. Since the sampling points located in the upper right of the injection tube are very close to that region, changing the grid size has a considerable effect on computational accuracy. Therefore, one expects higher computational uncertainties for the sampling points located in regions with more complex airflow structure.

CONCLUSIONS

In this study, the capability of a CFD commercial software in simulating turbulent airflow as well as tracer gas diffusion in a generic half cabin was evaluated. Two different types of turbulence models were used to find the turbulent viscosity in the governing equations: unsteady Large Eddy Simulation (LES) and steady-state Reynolds Averaged Navier Stokes (RANS) methods. While LES predicts the temporal variations of airflow velocity, the steady-state RANS method predicts a steady-state value for the velocity. Through the comparisons, it was concluded that the LES at least is able to predict the range of velocity variations fairly well. Examining the three different $k-\varepsilon$ (standard, RNG and Realizable) indicated that, as expected, the errors associated with the RANS method are much more than that of LES. It was also recognized that among the above mentioned $k-\varepsilon$ model, the standard $k-\varepsilon$ underestimated the velocity value, and the RNG and realizable models overestimated the velocity data. The most accurate predictions among the three RANS models were achieved using the RNG model.

In order to monitor the velocity data in PIV measuring windows, two different approaches were employed. The first approach used velocity data at the center points of the PIV windows and the second method used the area-averaged velocity values of the PIV windows. The comparisons indicated that the area-averaged velocity value decreased the fluctuations in the velocity but the general behavior of predicted velocities did not change. Comparisons with the experimental data showed that the center point values had a better agreement with experimental measurements.

In the second part of this study, the effect of halving the cabin inlet nozzle height with the same airflow rate was studied. It was observed that although LES method gave a good estimation of the velocity data in the locations 1, 2, 4 and 5 of measuring windows, the agreement between the simulations and measurements was not as good in the other locations. A local refinement in grid size is recommended to get more accurate results in this region in the future study. Comparing to the cabin with the full-height nozzle, it was seen that by halving the nozzle height and consequently doubling the inlet velocity, the magnitude of flow velocities in locations 1 and 4 increased dramatically (by 100%). However, in locations 2 and 5, the increase in the velocity value was slight and almost negligible. It was also realized that the airflow located in location 3 that used to be almost stationary in the full-height nozzle case had the tendency of moving to the upper left corner of the cabin model.

In the last part of this study, the capability of commercial CFD software in simulating the tracer gas diffusion in the generic cabin model was examined. In the corresponding simulations, LES was used to solve the Navier Stokes equations. Using LES, the temporal variations in tracer gas concentration in the specified sampling points were predicted. Following the same procedure as used in experiments the predicted values were non-dimensionalized and compared with experimental data. Although excellent agreement was observed in some sampling points, the predictions had an average error of 23%.

ACKNOWLEDGEMENT

The authors would like to express their gratitude to Dr. C. H. Lin from Boeing Company for his valuable input in CFD simulations, and to Dr. P. A. Lebbin from the National Research Council of Canada for his kind assistant in analyzing the experimental data and test procedures. The authors also would like to thank Dr. J. Bennett from the National Institute for Occupational Safety and Health (NIOSH) for his technical assistance. The research was funded, in part, by the Kansas State University Targeted Excellence Program.

REFERENCES

Bird, B.R., W.E. Steward, E.N Lightfoot, 2001, "Transport Phenomena", 2nd Edition, John Wiley and Sons, NY.

Fluent 6.3 User's Manual Guide (http:/my.fit.edu/itresources/manuals/fluent6.3, visited April 12, 2010).

Garner, R.P., K.L. Wong, S.C. Ericson, A.J. Baker, J.A. Orzechowaki, 2004, "CFD Validation for Contaminant Transport in Aircraft Cabin Ventilation Fields," Report No. DOT/FAA/AM-04/7, U.S. Department of Transportation and Federal Aviation Administration, Office of Aerospace Medicine, Washington DC.

Launder, B.E., and D.B. Spalding, 1972,"Lectures in Mathematical Models of Turbulence," Academic Press, London, England.

Lebbin, P., 2006, "Experimental and Numerical Analysis of Air, Tracer Gas and Particulate Movement in a Large Eddy Simulation Chamber," PhD dissertation, Kansas State University. Manhattan, Kansas.

Lilly, D.K, 1966, "On the application of the eddy viscosity conceptin the internal subrange of turbulences," NCAR Manuscrip123.

Lin, C.H., R.H. Horstman, M.F. Ahlers, L.M. Sedgwick, K.H. Dunn, J.L. Topmiller, J.S. Bennett, and S. Wirogo, 2005a, "Numerical simulation of airflow and airborne pathogen transport in aircraft cabins - Part 1: Numerical simulation of the flow field," *ASHRAE Transactions,* Vol.111, pp:755-763.

Lin, C.H., R.H. Hortsman, M.F. Ahlers, L.M. Sedgwick, K.H. Dunn, J.L. Topmiller, J.S. Bennett, S. Wirogo, 2005, "Numerical Simulation of Airflow and Airborne Pathogen Transport in Aircraft Cabins- Part II: Numerical Simulation of Airborne Pathogen Transport," *ASHRAE Transactions*, Vol.111, pp: 764-768.

Lin, C.H., R.H. Hortsman, P.A. Lebbin, M.H. Hosni, B.W. Jones, B.T. Beck, 2006, "Comparison of Large Eddy Simulation Predictions with Particle Image Velocimetry Data for the Airflow in a Generic Cabin," *HVAC&R Special Issue*, Vol. 12, Number 3c. pp: 935-951.

Shih, T.H., W.W. Liou, A. Shabbir, Z. Yang, and J. Zhu., 1995, "A New $k-\varepsilon$ Eddy-Viscosity Model for High Reynolds Number Turbulent Flows - Model Development and Validation. *Computers Fluids*, Vol. 24, No.3, pp: 227-238.

Smagorinsky, J., 1963, "General circulation experiments with the primitive equations: I. The Basic Experiment,". Monthly *Weather Review,* Vol. 91, pp: 99-164.

Tu, J., G.H. Yeoh, C. Liu, 2008, "Computational Fluid Dynamics- A Practical Approach,", pp: 102-106, Butterworth-Heinemann, USA.

V. Yakhot and S.A. Orszag., 1986,"Renormalization Group Analysis of Turbulence: I. Basic Theory," *Journal of Scientific Computing*, Vol.1, No.1, pp: 1-51.

Werner. H. and H. Wengle, 1991, "Large Eddy Simulation of Turbulent Flow Over and Around a Cube in a Plate Channel," 8th *Symposium on Turbulent Shear Flows*, Munich, Germany, 1991.